Electronic Supplementary Information (ESI)

Nature of surface space charge layer on *undoped* $SrTiO_3$ (001)

Hojoon Lim[1, #], Chanyang Song[1, #], Minsik Seo[1], Dongwoo Kim[1], Moonjung Jung[1], Habin Kang[1], Seunghwan Kim[1], Kyung-Jae Lee[1], Youngseok Yu[2], Geonhwa Kim[3], Ki-jeong Kim[3, *], Bongjin Simon Mun[1, 4, *]

[1]Department of Physics and Photon Science, Gwangju Institute of Science and Technology, Gwangju 61005, Republic of Korea

[2]Research Center for Materials Analysis, Korea Basic Science Institute, Daejeon 34133, Republic of Korea

[3]Beamline Research Division, Pohang Accelerator Laboratory, Pohang 37674, Republic of Korea

[4]Center for Advanced X-ray Science, Gwangju Institute of Science and Technology, Gwangju 61005, Republic of Korea

[#] Equally contribute to this work

[*]Corresponding author; E-mail: kjkim@postech.ac.kr, bsmun@gist.ac.kr

1. Images of AFM topography before and after a deionized-water leaching and thermal annealing treatment on $SrTiO_3$ (001) surface

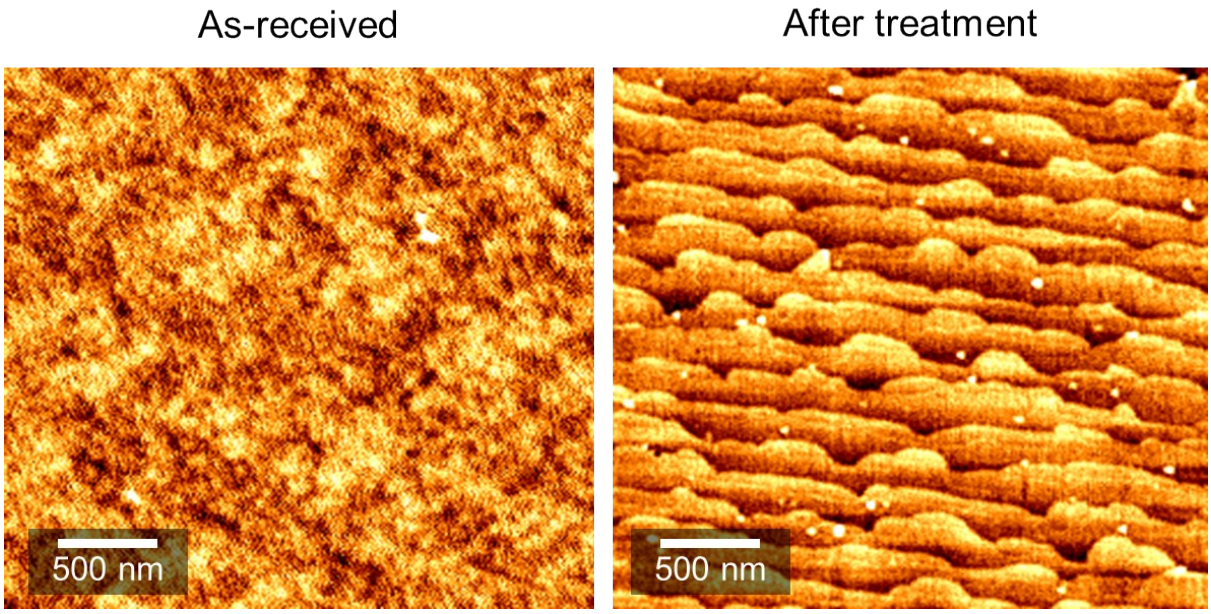

Figure S1. AFM topography images of $SrTiO_3$ (001) film for (left) as-received and (right) after 2 treatment cycles of a deionized-water leaching and thermal annealing treatment, *i.e.*, air annealing (1000℃, 1 hour) and DI water leaching (30 sec). An atomically flat and step-terraced surface structure can be seen on the right image.

2. Photon energy values for each probing depth and element

Element / Probing depth	O 1*s*	Ti 2*p*	C 1*s* & Sr 3*p*	Sr 3*d*
3.3 nm	920 eV	810 eV	710 eV	520 eV
2.4 nm	810 eV	710 eV	520 eV	380 eV
1.5 nm	710 eV	520 eV	380 eV	250 eV

Table S1. Photon energy values used for depth profiling of each element considering the formula of TPP 2M.[S1]

3. Band gap energy and conductivity of $SrTiO_3$ under both UHV and O_2 condition

Temperature (°C)	E_g (eV)	σ ($\Omega^{-1}cm^{-1}$) at UHV (10^{-9} mbar)	σ ($\Omega^{-1}cm^{-1}$) at O_2 0.1 mbar
600	2.90	~1.43×10^{-5}	~7.41×10^{-6}
500	2.99	~7.19×10^{-7}	~3.72×10^{-6}
400	3.05	~1.88×10^{-8}	~9.74×10^{-8}
300	3.12	~1.19×10^{-10}	~6.16×10^{-10}
200	3.17	~1.08×10^{-13}	~5.59×10^{-12}
100	3.24	~1.53×10^{-18}	~7.92×10^{-16}
0	3.28	~9.97×10^{-27}	~5.16×10^{-29}

Table S2. The band gap energies and conductivities of $SrTiO_3$ at each temperature under UHV (10^{-9} mbar) and O_2 (0.1 mbar) conditions calculated from the references.[S2, S3]

4. Apparent binding energy of C 1*s* before the energy calibration

	UHV			O_2 0.1 mbar		
	1.5 nm	2.4 nm	3.3 nm	1.5 nm	2.4 nm	3.3 nm
200°C	284.92 eV	285.51 eV	285.55 eV	284.43 eV	284.67 eV	285.04 eV
400°C	284.60 eV	284.58 eV	284.76 eV	283.61 eV	283.60 eV	283.87 eV
500°C	284.66 eV	284.64 eV	284.76 eV	-	-	-
600°C	284.60 eV	284.65 eV	284.72 eV	-	-	-

Table S3. C 1*s* binding energy of each pressure condition before the energy calibration. All C 1*s* binding energies are calibrated to 284.5 eV.[S4]

5. Characteristic core level spectra under both O_2 0.1 mbar and UHV condition

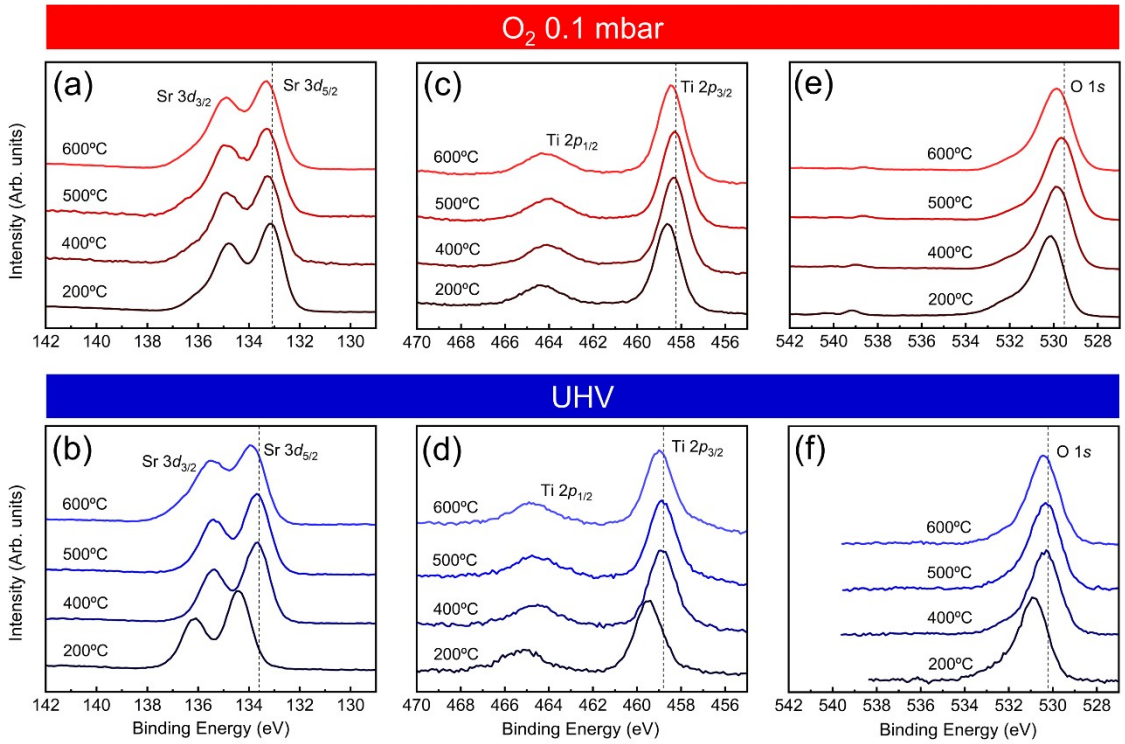

Figure S2. AP-XP spectra of $SrTiO_3$ (001) films during thermal annealing under both O_2 0.1 mbar [red series, (a), (c), (e)] and UHV [blue series, (b), (d), (f)] condition with the surface sensitive probing depth of 1.5 nm. Core level spectra of Sr 3*d* [(a), (b)], Ti 2*p* [(c), (d)], and O 1*s* [(e), (f)] are displayed for each annealing temperature step. The dotted vertical lines indicate the binding energy positions of $SrTiO_3$ lattice components at 500°C.

6. XPS fitting parameter for Sr 3*d* spectra under both O_2 and UHV condition

		Sr $3d_{5/2}$ (SrO_{1+x})		Sr $3d_{5/2}$ ($SrTiO_3$)	
		Binding energy (eV)	FWHM (eV)	Binding energy (eV)	FWHM (eV)
O_2 0.1 mbar	200℃	133.88	1.39	133.05	1.00
	400℃	133.93	1.60	133.12	1.07
	500℃	133.97	1.67	133.16	1.10
	600℃	133.99	1.62	133.18	1.13
UHV	200℃	135.00	1.10	134.37	1.14
	400℃	134.36	1.09	133.65	1.11
	500℃	134.39	1.18	133.64	1.15
	600℃	134.58	1.48	133.76	1.11

Table S4. Spectral fitting parameters for Sr 3*d* AP-XP spectra in Fig. 1(b) and (c). Binding energy positions of SrO_{1+x} and $SrTiO_3$ component are referenced in Ref. (S5).[S5] Full width half maximum (FWHM) values and separations of doublets at each gaseous environment are referenced in Ref. (S6).[S6]

7. Comparison of surface chemical states under both O_2 and UHV condition at 600℃

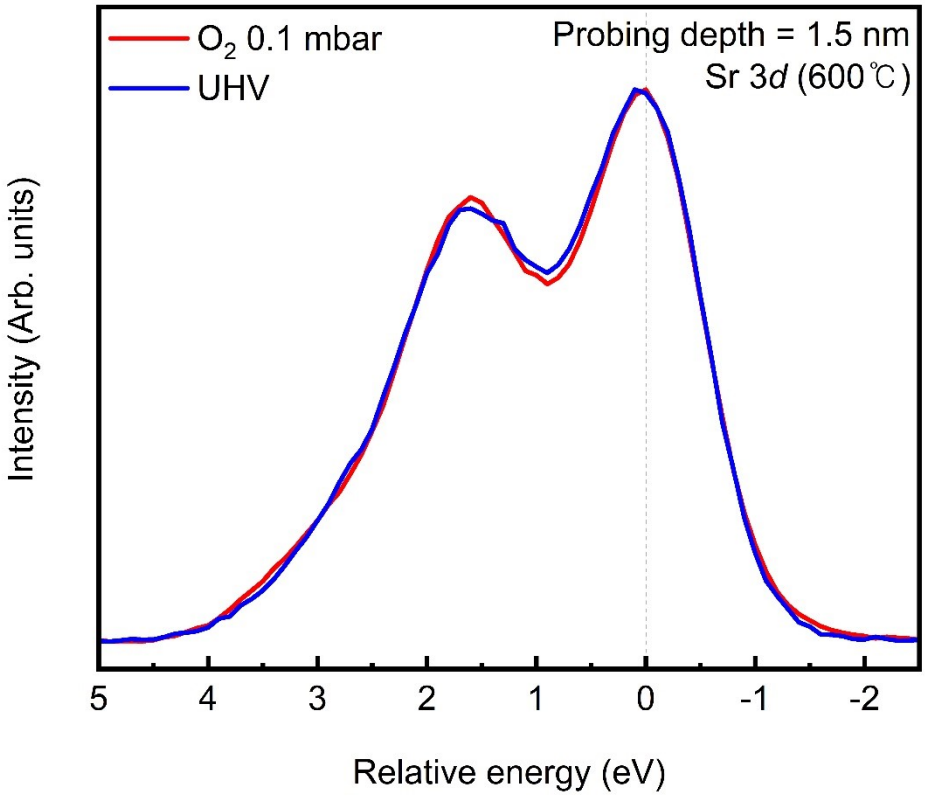

Figure S3. AP-XP spectra of Sr 3*d* obtained at 600℃ with probing depth of 1.5 nm during both O_2 (red) and UHV (blue) condition. To compare spectral shapes, Sr 3*d* spectra are superimposed to binding energy positions for $SrTiO_3$ lattice peaks. Sr 3*d* spectra under both conditions are almost identical, showing the formation of the same *surface chemical states* under both conditions.

8. Comparison of spectral shapes under both O_2 0.1 mbar and UHV condition

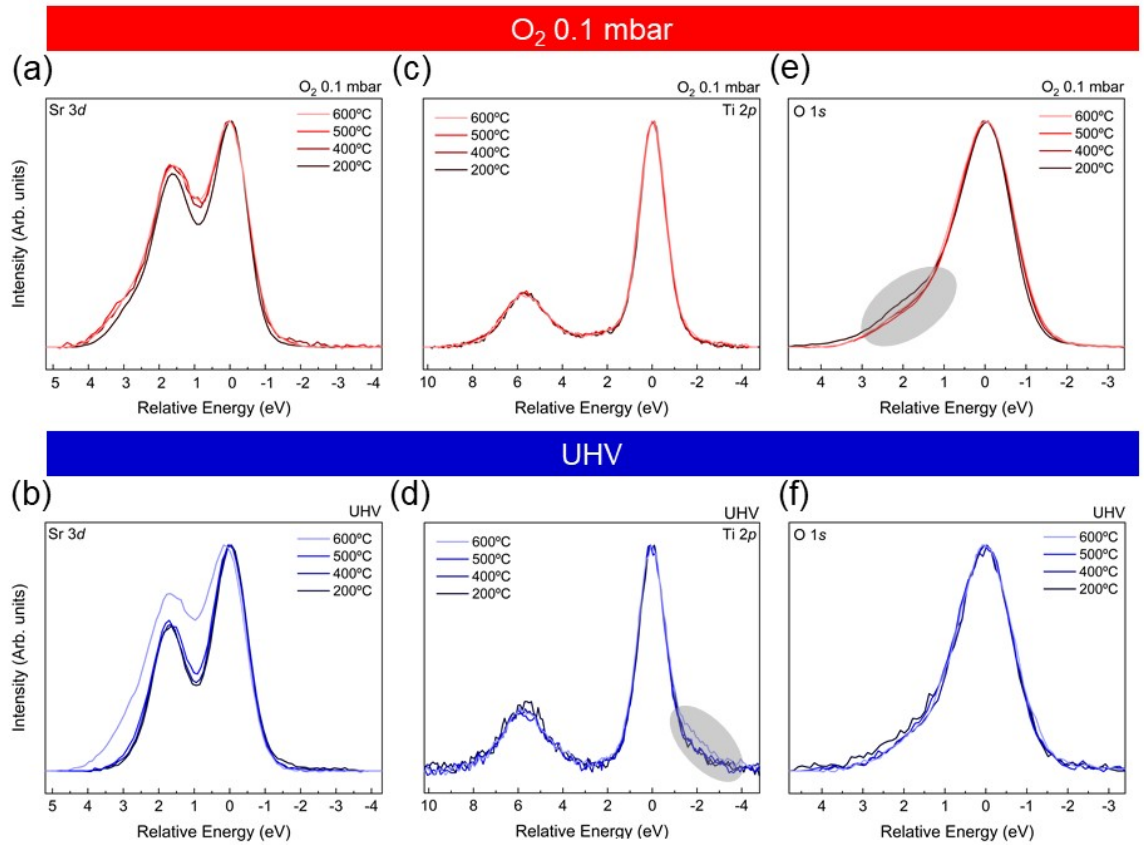

Figure S4. Entire set of spectra in Fig. S2 are superimposed on the binding energy positions of $SrTiO_3$ lattice peaks. For Sr 3*d* spectra, the formation of SrO_{1+x} surface oxide is clearly observed under both annealing conditions as discussed in this report. In Ti 2*p* spectra of (d), gray shaded area reveals emergence of Ti^{3+} component and formation of O vacancy (V_O) only during UHV annealing process. During O_2 annealing, spectral weight corresponding to hydroxide is reduced, shown in (e).

9. Sign of O vacancy formation under UHV in valence band region

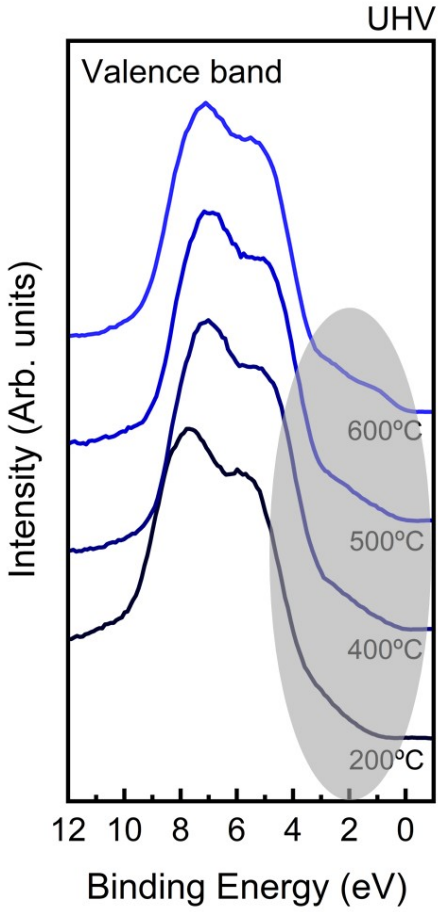

Figure S5. Valence band (VB) spectra of $SrTiO_3$ (001) film at probing depth of 1.5 nm under UHV condition during annealing from 200°C up to 600°C. During annealing in UHV, TiO_2 layer in $SrTiO_3$ are gradually reduced, *i.e.*, the formation of V_O. This feature is clearly visible in the gray shaded area by the enhancement of spectral weight as temperature increases, which is in good agreement with previous report.[S7]

10. Binding energy offsets between both O_2 and UHV condition

	O 1s			Ti $2p_{3/2}$			Sr $3d_{5/2}$			Averaged Δ
	UHV	O_2 0.1 mbar	Δ (UHV – O_2 0.1 mbar)	UHV	O_2 0.1 mbar	Δ (UHV – O_2 0.1 mbar)	UHV	O_2 0.1 mbar	Δ (UHV – O_2 0.1 mbar)	
200℃	530.87	530.12	0.75	459.50	458.62	0.88	134.37	133.05	1.32	0.98
400℃	530.29	529.80	0.49	458.84	458.34	0.50	133.65	133.12	0.53	0.51
500℃	530.27	529.61	0.66	458.82	458.30	0.52	133.64	133.16	0.48	0.55
600℃	530.37	529.83	0.54	458.97	458.44	0.53	133.76	133.18	0.58	0.55

Table S5. Characteristic binding energy positions of O 1*s*, Ti $2p_{3/2}$, and Sr $3d_{5/2}$ as a function of annealing temperature in Fig. 4(a). The Δ values, the binding energy offset values between UHV and O_2 conditions, are calculated for each temperature and each core level. In particular, the Δ values at temperatures above 400℃, when charging effect is completely compensated, are displayed in blue (400°C), orange (500°C), and red (600°C), respectively. The averaged Δ values at the rightmost of the table are the average values of the binding energy offset values at each temperature, *i.e.*, average of Δ values of O 1*s*, Ti $2p_{3/2}$, and Sr $3d_{5/2}$. At temperatures above 400°C, the binding energy offset values are almost constant, ~0.54 eV on average, signaling the band bends upward by ~0.54 eV during O_2 annealing.

11. Observation of upward band bending under O_2 annealing in valence band spectra

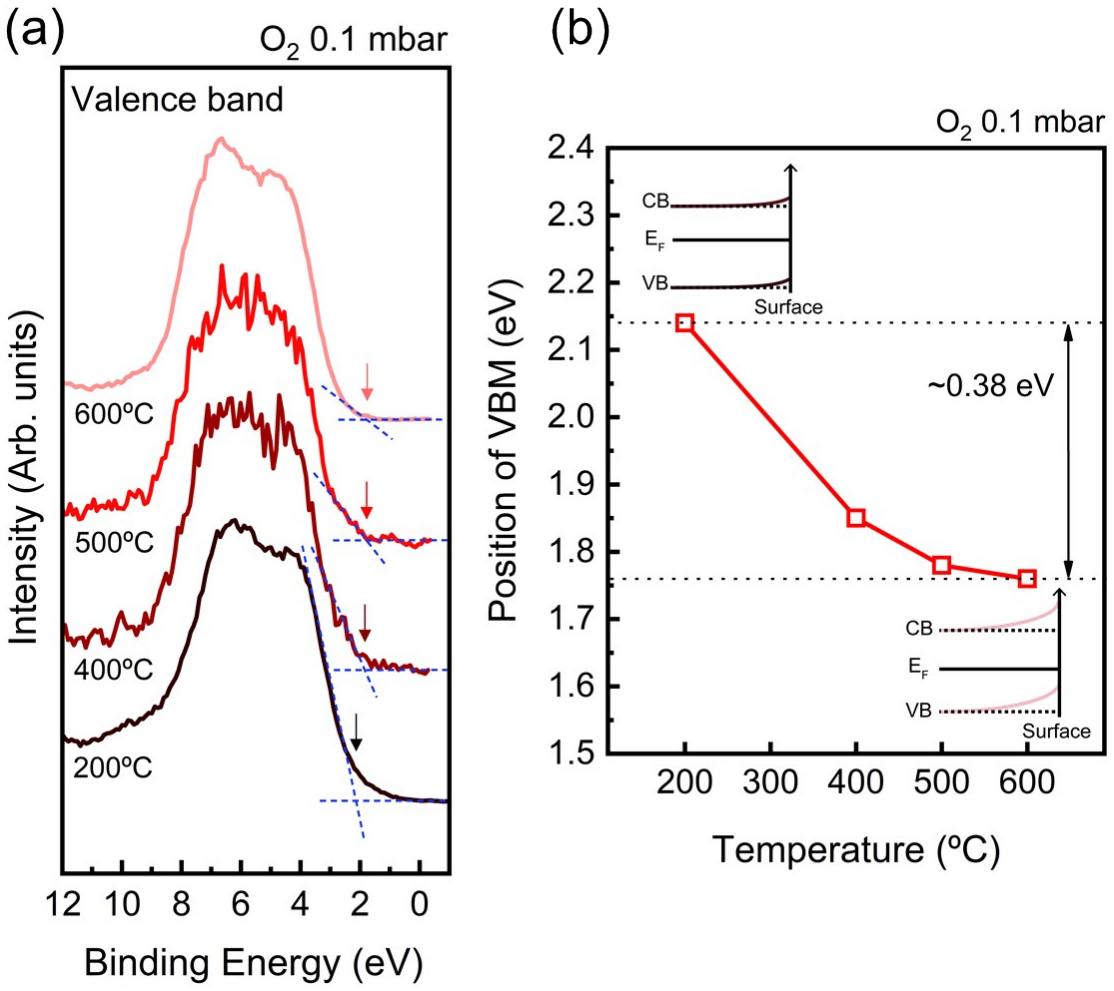

Figure S6. (a) VB spectra of $SrTiO_3$ (001) film at probing depth of 1.5 nm and O_2 pressure of 0.1 mbar during annealing from 200°C up to 600°C. The position of valence band maximum (VBM) is determined as the intersection of the leading edge (blue dotted line) of the VB spectra and background. The positions of VBM as a function of annealing temperature are plotted in (b). As annealing temperature increases up to 600°C, the position of VBM is shifted from 2.14 eV to 1.76 eV. This means that as the annealing temperature increases during the O_2 annealing process, the formation of surface space charge layer and upward band bending become more pronounced.

12. Calculation of Debye length

The discussion of space charge layer is only valid when Debye length is bigger than the scales of the space charge layer. Therefore, in order to discuss the formation and characteristics of the space charge layer by charge separation, the Debye length is calculated and compared.

Debye length of a material L_D can be given as[S8]:

$$L_D = \sqrt{\frac{\varepsilon_0 \varepsilon_r k_B T}{e^2 n}}$$

where, ε_0: permittivity of free space (~ 8.85×10^{-12} F·m^{-1})

ε_r: dielectric constant

k_B: Boltzmann constant (~ 1.38×10^{-23} J·K^{-1})

T: temperature of a material

e: elementary charge (~ 1.60×10^{-19} C)

n: charge density

	ε_r	n (m^{-3})	L_D (m)
600°C	~ 4630	~ 1.13×10^{22}	~ 1.31×10^{-6}
500°C	~ 3220	~ 5.05×10^{20}	~ 4.84×10^{-6}
400°C	~ 2020	~ 4.24×10^{17}	~ 1.24×10^{-4}
300°C	~ 510	~ 2.19×10^{13}	~ 7.98×10^{-3}
200°C	~ 180	~ 1.70×10^{7}	~ 4.89
100°C	~ 200	~ 3.50×10^{-3}	~ 3.19×10^{5}
0°C	~ 240	~ 8.95×10^{-20}	~ 5.91×10^{13}

Table S6. Dielectric constant (ε_r) and charge density (n) values of $SrTiO_3$ as a function of temperature.[S9, S2, S3] Charge density values are calculated by extrapolation from the references[S2, S3], and Debye length is calculated by substituting the dielectric constant and charge density values at each temperature into the above formula.

As can be seen from Table S6, the thickness of the space charge layer within our probing depth (< 3.3 nm) is much smaller than Debye length. Therefore, our discussion on the nature of space charge layer is valid.

References

S1 S. Tanuma, C. J. Powell and D. R. Penn, *Surf. interface Anal.*, 1994, **21**, 165–176

S2 T. Bieger, J. Maier, R. Waser, *Solid State Ionics.*, 1992, **53–56**, 578–582.

S3 R. C. Hatch, M. Choi, A. B. Posadas, A. A. Demkov, *J. Vac. Sci. Technol. B, Nanotechnol. Microelectron. Mater. Process. Meas. Phenom.*, 2015, **33**, 061204.

S4 J. F. Moulder, W. F. Stickle, P. E. Sobol and K. D. Bomben, *Handbook of X-ray Photoelectron Spectroscopy*, United States of America, 1993.

S5 R. C. Hatch, M. Choi, A. B. Posadas, A. A. Demkov, *J. Vac. Sci. Technol. B, Nanotechnol. Microelectron. Mater. Process. Meas. Phenom.*, 2015, **33**, 061204.

S6 G. M. Vanacore, L. F. Zagonel, N. Barrett, *Surf. Sci.*, 2010, **604**, 1674–1683.

S7 R. C. Hatch, K. D. Fredrickson, M. Choi, C. Lin, H. Seo, A. B. Posadas, A. A. Demkov, *J. Appl. Phys.*, 2013, **114**, 103710.

S8 W. Mönch, *Electronic Properties of Semiconductor Interfaces*, Springer-Verlag Berlin Heidelberg, 2004

S9 N. F. Muhamad, R. A. M. Osman, M. S. Idris, M. N. M. Yasin, *EDP Sciences*, 2017, **162**, 01052